Ocular dominance-dependent binocular combination of monocular neuronal responses in macaque V1

Sheng-Hui Zhang[1*], Xing-Nan Zhao[1*], Shi-Ming Tang[1,2,3#], & Cong Yu[3,4#] Sept. 16, 2023

[1]PKU-Tsinghua Center for Life Sciences, [2]School of Life Sciences, [3]IDG-McGovern Institute for Brain Research, and [4]School of Psychological and Cognitive Sciences, Peking University, Beijing, China

* Equal-contribution first authors.

Correspondence authors: Shi-Ming Tang (tangshm@pku.edu.cn) & Cong Yu (yucong@pku.edu.cn)

Abstract

Primates rely on two eyes to see depth, while keeping a stable vision when one eye is closed. Although psychophysical and modeling studies have investigated how monocular signals are combined to form binocular vision, the corresponding neuronal mechanisms, especially in V1 where most neurons become binocular but with different eye preferences, are not well understood. Here we used two-photon calcium imaging to compare monocular and binocular responses of thousands of V1 superficial-layer neurons in three awake macaques. Under monocular stimulation, neurons preferring the stimulated eye responded substantially stronger than those preferring both eyes. However, under binocular stimulation, the responses of neurons preferring either eye were suppressed, and those preferring both eyes were enhanced, so that neuronal responses became similar regardless of eye preferences. A neuronally realistic model of binocular combination, which includes ocular dominance-dependent divisive interocular inhibition, and binocular summation, is proposed to account for these observations.

Introduction

Human and non-human primates often use binocular disparity, or the differences between the retinal images of two eyes, to perceive depth (stereopsis). In the meantime, the brain maintains a stable perception of the visual world when one eye closes and the incoming light is halved. Much has been known regarding the neural foundations of stereopsis (Barlow, Blakemore, & Pettigrew, 1967; Henriksen, Tanabe, & Cumming, 2016; Parker, Smith, & Krug, 2016; Welchman, 2016; Read, 2021). Nevertheless, whether and how the neurons respond differently to monocular and binocular stimulations is less studied (Prince, Pointon, Cumming, & Parker, 2002; Dougherty, Cox, Westerberg, & Maier, 2019; Mitchell et al., 2022). Adding to the complexity is the fact that many V1 neurons, although responding to stimulations in both eyes, have various degrees of eye preferences (Hubel & Wiesel, 1962, 1968). Thus, a more complete picture of binocular combination of monocular responses would illustrate monocular and binocular responses of neurons at different eye preferences, which is the purpose of the current study.

It has been reported that overall the binocular responses of macaque V1 neurons are lower than the sum of monocular responses to each eye (Prince et al., 2002; Mitchell et al., 2022), but are stronger than monocular responses either when one eye was stimulated (Prince et al., 2002; Mitchell et al., 2022), or when neurons' preferred eye was stimulated (Mitchell et al., 2022). Further, Dougherty et al. (2019) reported that the responses of monocular neurons are found to be more likely suppressed than facilitated by binocular stimulation. As our results will suggest later, this conclusion is valid when the monocular baseline is either the sum of monocular responses, or the monocular responses of either eye. Dougherty et al. (2019) also reported similar responses of neurons with monocular and binocular preferences, as well as similar responses of binocular neurons to monocular and binocular stimulations, which are not supported by our data.

A big and more complete picture of the binocular combination of monocular responses, as well as the impacts of eye preferences, would come from large samples of neurons, so that the data can be quantitatively described with sufficient statistical power, and analyzed with computational modeling. Two-photon calcium imaging is capable of recording thousands of neurons simultaneously at the single-neuron resolution, which is especially suitable for this task. In this study, we used a two-photon imaging setup, which had been adapted for recording with awake macaques (Li, Liu, Jiang, Lee, & Tang, 2017), to measure responses of V1 superficial-layer neurons to monocular and binocular stimulations. Furthermore, a neuronally realistic binocular combination model, which considers ocular dominance-dependent interocular divisive inhibition, as well as binocular summation, is proposed to explain the data.

Results

We recorded responses of V1 superficial-layer neurons to monocular (contralateral and ipsilateral) and binocular stimulations in three awake, fixating macaques. The stimulus was a high-contrast (0.9) Gabor grating at various orientations and spatial frequencies (SFs). The recording was performed at two cortical depths of the same response field of view (FOV) in first two monkeys (MA & MB), and at one depth in the third monkey (MC) as the first two monkeys displayed similar results at two depths (Fig. 1A). Imaging processing identified a total of 10,168 neurons. Among them, 9,390 (92.4%) were tuned to orientation, SF, or both. Results from these orientation- and/or SF-tuned neurons were used in the following data analysis.

V1 superficial-layer neurons exhibited various degrees of eye preferences, consistent with the classical findings of Hubel and Wiesel (1962, 1968). An ocular dominance index (ODI) was calculated to characterize each neuron's eye preference: ODI = $(R_i - R_c)/(R_i + R_c)$, in which R_i and R_c were the neuron's respective peak responses to ipsilateral and contralateral stimulations on the basis of data fitting (see Methods). Here ODI = -1 and 1 would indicate complete contralateral and ipsilateral eye preferences, respectively, and ODI = 0 would indicate equal preferences to both eyes. The ocular dominance functional maps at single-neuron resolution, especially those of Monkeys A and C, showed regions of neurons preferring either the contralateral (blue) or the ipsilateral eye (red), and transitional zones where neurons preferring both eyes (white) (Fig. 1B). The ocular dominance maps were similar at two cortical depths in Monkeys A and B, indicating possible ocular dominance columns (Fig. 1B). The frequency distributions of ODIs suggest more binocular neurons than monocular neurons in V1 superficial layers (Fig. 1C), similar to the normal distribution of ocularity index in Dougherty et al. (2019).

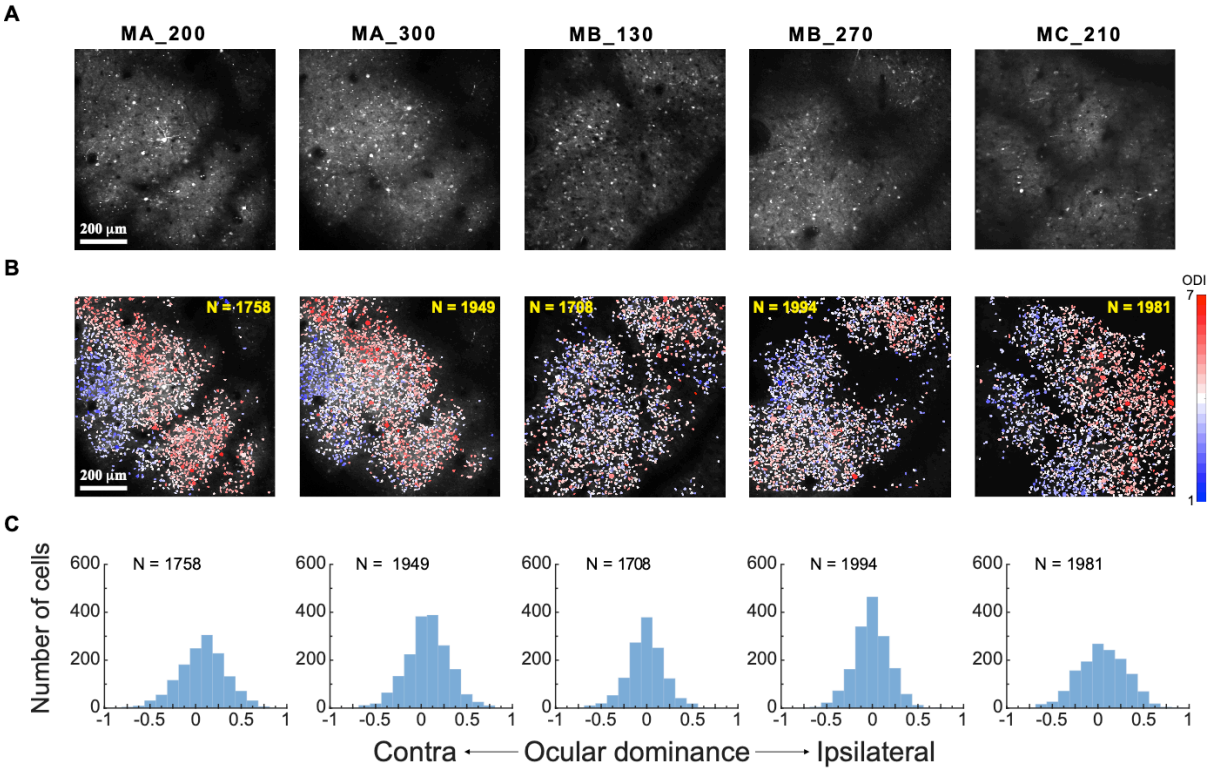

Figure 1. Eye preferences of V1 superficial-layer neurons in three macaques. **A**. Two-photon imaging. Average 2-photon images over a recording session for each response FOV. MA_200: Monkey A at a 200-µm cortical depth. **B**. Ocular dominance functional maps of each FOV/depth at single-neuron resolution. **C**. Frequency distributions of neurons of each FOV/depth as a function of ocular dominance index.

The responses of individual neurons were plotted against the ocular dominance index (ODI) when monocular stimulation was through the contralateral eye (Fig. 2A) or the ipsilateral eye (Fig. 2B). As expected, neurons with more negative ODIs responded stronger when the contralateral eye was stimulated, and those with more positive ODIs responded stronger when the ipsilateral eye was stimulated. The responses declined as neurons became more binocular. However, when both eyes were stimulated, the response differences among neurons of different eye preferences became not obvious (Fig. 2C).

These trends can be better appreciated when the difference between binocular and monocular responses are presented for each FOV/depth in Fig. 2D: Under monocular stimulation, if only the neuronal responses to the preferred eye were taken into consideration (i.e., a neuron's higher response to ipsilateral vs. contralateral stimulations), more monocular neurons (ODIs farther from 0) tended to have stronger responses than more binocular neurons (ODIs closer to 0). However, under binocular stimulation, the responses of more monocular neurons were suppressed, and those of more binocular neurons were enhanced, by binocular stimulation. These trends are best appreciated in pooled data over five FOVs/depths (Fig. 2E). Further, linear regression confirmed a significant dependence of binocular modulation on absolute ODI ($y = -0.41x + 0.16$, $p < 0.001$) (Fig. 2E). That is, responses of neurons with lower absolute ODI (i.e., binocular neurons) tended to be more enhanced, and responses of neurons with higher absolute ODI (i.e., monocular neurons) tended to be more suppressed.

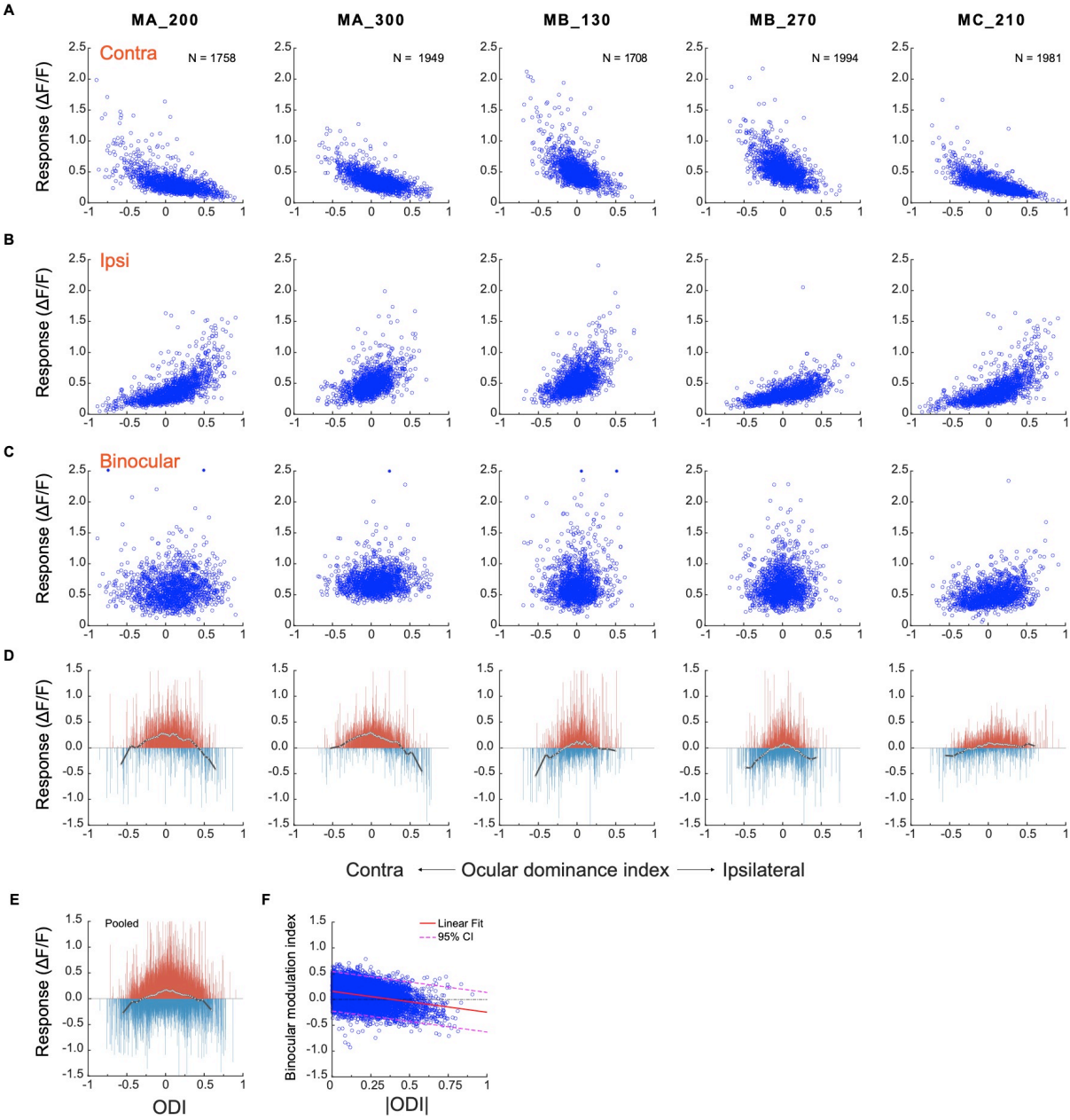

Figure 2. A comparison of neuronal responses to monocular and binocular stimulations. **A**. Responses of individual neurons against their ocular dominance indices with contralateral stimulation. **B**. Responses of the same neurons against their ocular dominance indices with ipsilateral stimulation. **C**. The binocular responses of the same neurons. **D**. The difference between binocular and monocular responses (R_b – max(R_i, R_c)). Each vertical line represents one neuron. To summarize the results, neurons of each FOV/depth are evenly divided into 60 bins in the order of the ocular dominance index. White dots represent the median responses

119 of respective bins and are connected with a black line. **E**. The differences between binocular
120 and monocular responses of individual neurons pooled over five FOVs/depths. **F**. Binocular
121 modulation index as a function of absolute ODI and the linear fit. The binocular modulation
122 index of each neuron was defined as $(R_b - \max(R_i, R_c))/(R_b + \max(R_i, R_c))$.
123
124 *Modeling monocular and binocular responses*
125 To model the monocular and binocular neural responses, monocular and binocular
126 data of each FOV/depth, as well as the pooled data, were first normalized by the respective
127 median of the binocular responses and then divided into 60 bins in the order of the ocular
128 dominance index (Fig. 3A-C).
129 Monocular responses
130 A neuron's monocular responses to contralateral and ipsilateral stimulations could be
131 respectively described by a divisive gain control model:
132 $$R_c = \frac{w_c^{m_c} \cdot S_c}{k} \quad \text{and} \quad R_i = \frac{w_i^{m_i} \cdot S_i}{k} \qquad \text{(Eq. 1)}$$
133 Here S_c and S_i were stimulus contrasts, w_c and w_i were linear transformations of a neuron's
134 ocular dominance index from [-1 1] to [0 1]: $w_c = (ODI + 1)/2$ and $w_i = 1 - w_c$, m_c and m_i
135 represented monocular nonlinearity, and k represented divisive gain control. Because S_c and
136 S_i in our experiments were 0.9, which were about equal to 1 (full contrast) due to neuronal
137 response saturation, the above equations were simplified as
138 $$R_c = \frac{w_c^{m_c}}{k} \quad \text{and} \quad R_i = \frac{w_i^{m_i}}{k} \qquad \text{(Eq. 2)}$$
139 Eq. 2 was used to fit the binned median contralateral and ipsilateral data (Figs. 3A &
140 B), with the parameter k being equal for contralateral and ipsilateral responses. The fitting

141 revealed that m_c and m_i were negative and close to -1, which resulted in a quick decline of

142 $w_c^{m_c}$ and a quick increase of $w_i^{m_i}$ as a function of the ocular dominance index since w_c and

143 $w_i \in [0, 1]$. The fit quality indices (Busse, Wade, & Carandini, 2009) ranged 0.85-0.95 for the

144 contralateral condition (Fig. 3A) and 0.90-0.93 for the ipsilateral condition (Fig. 3B),

145 suggesting adequate goodness of fit. The fitting parameters are listed in Fig. 3D.

146 Binocular responses

147 Fig. 2D-F earlier has indicated that neuronal responses to binocular stimulation

148 change from suppression to enhancement as neurons' ocular dominance changes from

149 monocular to binocular, which may reflect the ocular dominance-dependent net effect of

150 interocular suppression and binocular summation. To model interocular response

151 suppression, responses from each eye in Eq. 2 were further normalized by an interocular

152 suppression factor w_i^b or w_c^b, whose strength was decided by the linearly transformed ODI

153 with a nonlinear exponent b. Then the normalized responses from two eyes were summed

154 to model binocular summation and the final binocular responses of neurons R_b (Eq. 3).

155 $$R_b = \frac{w_i^{m_i}}{kw_i^b} + \frac{w_c^{m_c}}{kw_c^b} \qquad \text{(Eq. 3)}$$

156 During data fitting, the parameters m_i, m_c, and k were inherited from earlier

157 monocular data fitting and remained fixed. Only b was allowed to change. Data fitting

158 resulted in flat binocular response functions (Fig. 3C) with satisfactory goodness-of-fit (fit

159 quality index = 0.86 to 0.94).

160

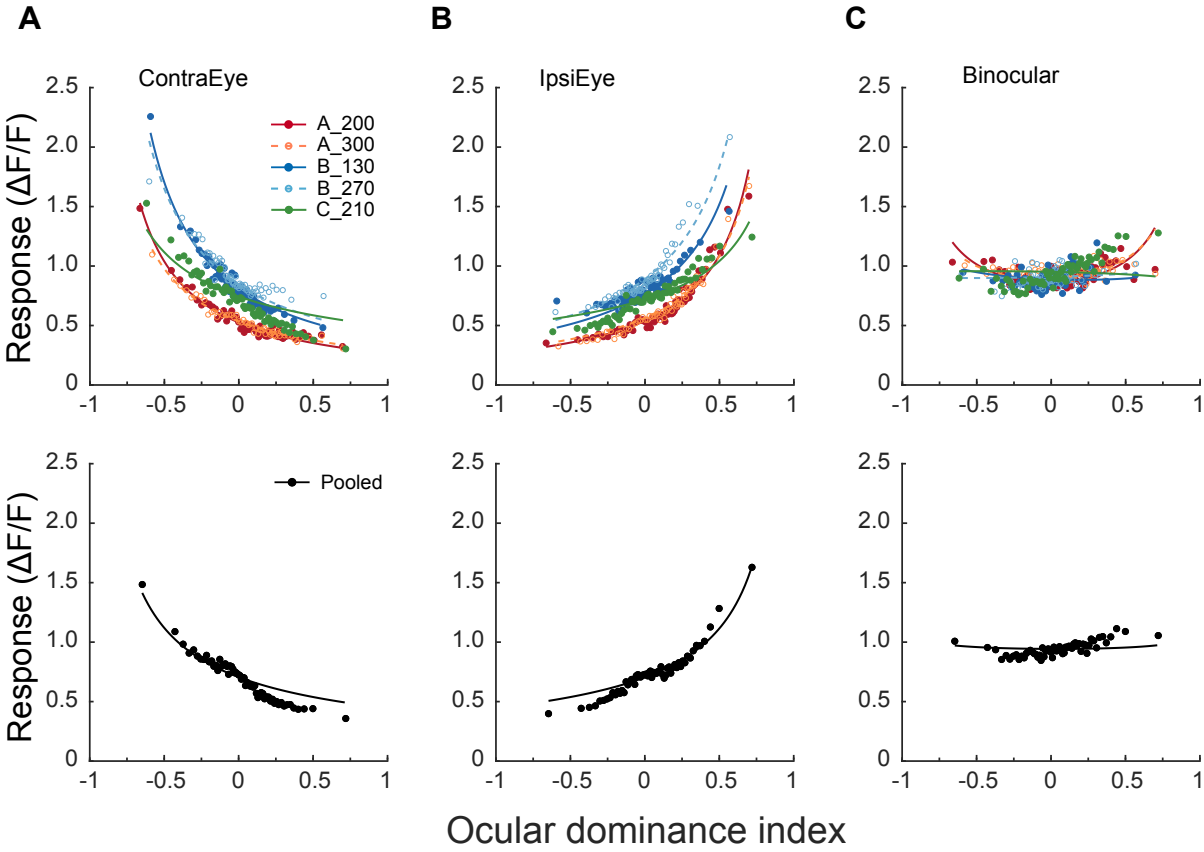

D

	m	k		m	k		b
A_200	-0.981	3.717		-1.008	3.717		0.302
A_300	-0.868	3.380		-0.936	3.380		0.302
B_140	-1.074	2.582		-0.984	2.582		0.825
B_250	-0.967	2.299		-1.036	2.299		0.935
C_210	-0.585	2.005		-0.532	2.005		0.622
Pooled	-0.672	2.270		-0.665	2.270		0.578

Figure 3. Modeling monocular and binocular responses. **A & B**. Median neuronal responses to contralateral and ipsilateral stimulations as a function of ocular dominance index and respective data fitting with Eq. 2. Neurons are evenly divided into 60 bins in the order of the ocular dominance index, with each bin containing 28-33 neurons that varied among different FOVs/depths (156 neurons for the pooled data). Each datum represents the median response of a bin. Free parameter k was kept equal during contralateral and ipsilateral data fitting. **C**. Binocular responses as a function of ocular dominance index and data fitting with Eq. 3 for the same bins of neurons. During binocular data fitting, parameters k, m_i, and m_c

170 were inherited from monocular data fitting, and only b was the free-changing parameter. **D**.
171 The values of free parameters from monocular and binocular data fitting.
172
173 The behaviors of interocular suppression and binocular summation in the model, as
174 well as their contributions to the binocular response, may be better appreciated in Fig. 4. Fig.
175 4A uses Eqs. 2 and 3 and the parameters from fitting of pooled data (Fig. 3D) to simulate the
176 contralateral (blue curve with label R_c), ipsilateral (red curve with label R_i), and binocular
177 (black curve) response functions against the ocular dominance index. The arithmetic sum of
178 contralateral and ipsilateral response functions was also simulated (grey dashed curve
179 labeled $R_i + R_c$). In addition, neuronal responses to preferred eye stimulation would consist of
180 the higher branches of contralateral and ipsilateral response functions. It is apparent that
181 binocular responses can be described by neither the sum of monocular responses, nor the
182 responses to the preferred eye. Instead, the median of the binocular response function
183 (black arrow) in each data set is close to but still more or less higher than the median of the
184 contralateral (blue arrow) or ipsilateral response function (red arrow), which is consistent
185 with previous reports (Prince et al., 2002; Mitchell et al., 2022).
186 Fig. 4B plots the interocular suppression factor w_c^b (dotted blue curve) for the
187 contralateral response R_c (solid blue curve from 4A), and w_i^b (dotted red curve) for the
188 ipsilateral response R_i (solid red curve from 4A). The suppression factors w_c^b and w_i^b are
189 larger with neurons that are more monocular than with neurons that are more binocular. The
190 R_c and R_i are divided by the respective interocular suppression factor, producing the
191 normalized contralateral responses (dashed blue curve labeled R_c/w_c^b) and ipsilateral
192 responses (dashed red curve labeled R_i/w_i^b). These normalized curves are lower than original

monocular responses, especially for neurons that are more monocular (ODIs farther from 0), showing interocular suppression.

Then the normalized monocular curves are summed up in Fig. 4C, which represents binocular summation and produces the final binocular responses (R_b). Therefore, as a result of combined interocular suppression and binocular summation, the final curve for binocular responses becomes nearly flat within the data range.

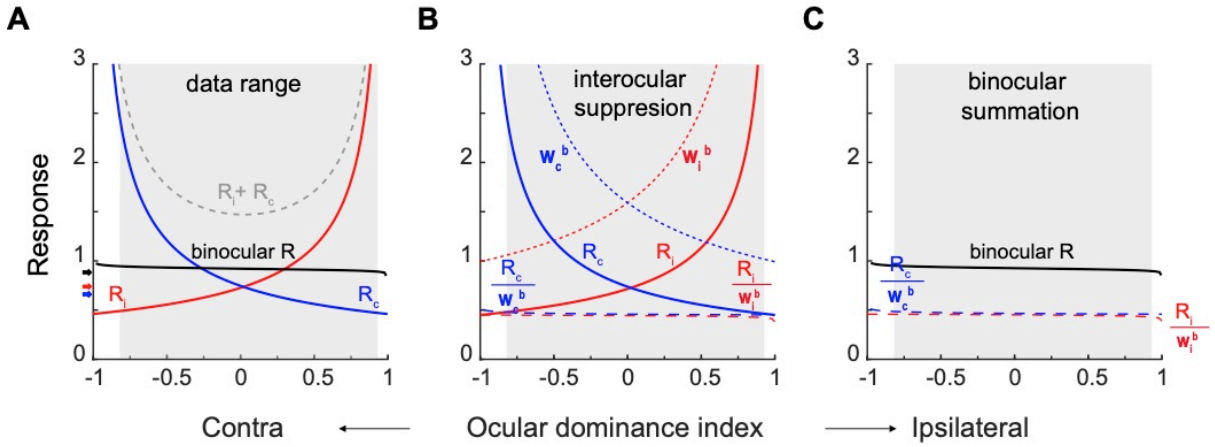

Figure 4. Monocular and binocular responses modeled with binocular suppression and binocular summation. **A.** The solid blue, red, and black curves are simulations of the contralateral, ipsilateral, and binocular responses on the basis of fitting of pooled data (Fig. 3D). The grey dashed curve simulates binocular responses as the arithmetic sum of contralateral and ipsilateral responses. The higher branches of contralateral and ipsilateral response functions represent monocular responses with preferred eye stimulation. The black, blue, and red arrows indicate the median binocular, contralateral, and ipsilateral responses, respectively, from pooled data. The shadowed area indicates the region where actual neurons existed on the basis of the ocular dominance index. **B.** Interocular suppression. The contralateral and ipsilateral responses (R_c & R_i) are divided by respective interocular suppression factors W_c^b and W_i^b to produce interocular-suppressed responses R_c/w_c^b and R_i/w_i^b. **C.** Binocular summation. R_c/w_c^b and R_i/w_i^b are summed to produce the final binocular responses R_b.

Discussion

The current study compared the responses of large samples of V1 superficial-layer neurons to monocular and binocular stimulations in three macaques. The monocular response functions show steep changes as a function of the ocular dominance index, but binocular response functions are largely flat, regardless of neurons' eye preferences. Modeling efforts indicated that when signals from two eyes are combined, interocular divisive suppression, which is more prominent with neurons preferring one eye, and binocular summation, which is more prominent with binocular neurons, together produce the nearly flat binocular response function within a broad range of ocular dominance indices.

As shown in Fig. 4A, the median of binocular neuronal responses is slightly higher than that of monocular responses of either eye (black vs. red/blue arrows), consistent with earlier reports (Prince et al., 2002; Mitchell et al., 2022). However, individually, compared to monocular responses, responses of monocular neurons more preferring the stimulated eye are actually suppressed, and only responses of binocular neurons are increased by binocular stimulation. Furthermore, overall stronger binocular than monocular responses in V1, even with a small amount, would suggest that the binocular neuronal responses must be further modulated by additional mechanisms to achieve stable vision, regardless of whether the world is viewed with one or two eyes.

In Dougherty et al. (2019), the responses of monocular and binocular neurons are similar under monocular stimulation, and only monocular neurons, but not binocular neurons, are significantly suppressed by binocular stimulation. In contrast, our results show that monocular neurons respond to stimulation in the preferred eye much more strongly than binocular neurons do to the same monocular stimulation (Fig. 2C). Moreover, although

237 confirming interocular suppression of monocular neurons responding to the preferred eye,
238 our results also indicate enhanced responses of binocular neurons to binocular stimulation.
239 Considering the large diversity of binocular responses of neurons with similar eye
240 preferences (Fig. 2C), it is very possible to obtain inaccurate statistical estimates with small,
241 and possibly biased, samples of neurons in electrode recording experiments.

242 Binocular combination of monocular signals has long been recognized to involve both
243 interocular suppression and binocular summation (DeSilva & Bartley, 1930; Cohn & Lasley,
244 1976; Li & Atick, 1994). Most more recent models use divisive normalization to explain
245 interocular suppression (e.g., Cogan, 1987; Anderson & Movshon, 1989; Ding & Sperling,
246 2006; Moradi & Heeger, 2009; Huang, Zhou, Zhou, & Lu, 2010; Ding, Klein, & Levi, 2013). Our
247 modeling effort shows that a similar divisive interocular suppression and binocular
248 summation model can account for neuronal response changes under monocular and
249 binocular stimulations, with the distinction that the divisive interocular suppression is
250 additionally controlled by a neuron's ocular dominance. The latter also controls the
251 responses of individual neurons to monocular stimulation, as shown in Figs. 3A-B. The critical
252 roles of ocular dominance have been largely overlooked by extant binocular vision models to
253 our knowledge, except that Anderson and Movshon (1989) demonstrated that a model
254 consisting of multiple ocular dominance channels can better explain their psychophysical
255 adaptation data. We hope that our two-photon imaging results can be incorporated into
256 future neuronally plausible models of binocular vision.

257 On the basis of current findings, future two-photon imaging work shall compare
258 neural responses to monocular and binocular stimulations with uneven effective stimulus
259 contrasts due to physical contrast differences (Anderson & Movshon, 1989), monocular
260 adaptation (Anderson & Movshon, 1989), and short-term monocular deprivation (Lunghi,

261 Burr, & Morrone, 2011), as well as the relevant roles of ocular dominance of individual
262 neurons. These results would help understand abnormal binocular vision in patients with
263 strabismus and amblyopia. In addition, under current zero-disparity stimulus conditions,
264 neuronal responses to binocular stimulation appear no longer affected by ocular dominance
265 of individual neurons (Fig. 2D). Therefore, another interesting question is whether the same
266 is true when disparity is present in the stimuli. These future results would enrich and refine
267 our current simplified but neuronally realistic model.
268
269 **Materials and Methods**
270 *Monkey preparation*
271 Monkey preparations were identical to those reported in a previous study (Guan, Ju,
272 Tao, Tang, & Yu, 2021; Ju, Guan, Tao, Tang, & Yu, 2021). Three rhesus monkeys (*Macaca*
273 *mulatta*) aged 4 to 6 years, respectively, were each prepared with two sequential surgeries
274 under general anesthesia and strictly sterile condition. In the first surgery, a 20-mm diameter
275 craniotomy was performed on the skull over V1. The dura was opened and multiple tracks of
276 100-150 nL AAV1.hSynap.GCaMP5G.WPRE.SV40 (AV-1-PV2478, titer 2.37e13 (GC/ml), Penn
277 Vector Core) were pressure-injected at a depth of ~350 μm. Then the dura was sutured, the
278 skull cap was re-attached with three titanium lugs and six screws, and the scalp was sewn up.
279 After the surgery, the animal was returned to the cage, treated with injectable antibiotics
280 (Ceftriaxone sodium, Youcare Pharmaceutical Group, China) for one week. Postop analgesia
281 was also administered. The second surgery was performed 45 days later. A T-shaped steel
282 frame was installed for head stabilization, and an optical window was inserted onto the
283 cortical surface. Data collection could start as early as one week later. More details of the
284 preparation and surgical procedures can be found in Li et al. (2017). The procedures were

approved by the Institutional Animal Care and Use Committee, Peking University.

Behavioral task

After a ten-day recovery from the second surgery, monkeys were seated in primate chairs with head restraint. They were trained to hold fixation on a small white spot (0.1°) with eye positions monitored by an ISCAN ETL-200 infrared eye-tracking system (ISCAN Inc.) at a 120-Hz sampling rate (Monkeys A & B) or an Eyelink-1000 (SR Research) at a 1000-Hz sampling rate (Monkey C). During the experiment, trials with the eye position deviated 1.5° or more from the fixation before stimulus offset were discarded as ones with saccades and repeated. For the remaining trials, the eye positions were mostly concentrated around the fixation point, with eye positions in over 95% of trials within 0.5° from the fixation point. The viewing was binocular.

Visual stimuli

For Monkeys A and B, visual stimuli were generated by the ViSaGe system (Cambridge Research Systems) and presented on a 21'' Sony G520 CRT monitor (refresh rate = 80 Hz, resolution = 1280 pixel × 960 pixel, pixel size = 0.31 mm × 0.31 mm). Because of the space limit, the viewing distance and the monitor position varied depending on the stimulus spatial frequency (30 cm at 0.25, 0.5, and 1 cpd, 60 cm at 2 cpd, and 120 cm at 4 and 8 cpd). For Monkey C, visual stimuli were generated by Psychotoolbox 3 (Pelli & Zhang, 1991) and presented on a 27'' Acer XB271HU LCD monitor (refresh rate = 80 Hz native, resolution = 2560 pixel × 1440 pixel native, pixel size = 0.23 mm × 0.23 mm). The viewing distance was 50 cm for lower frequencies (0.25 - 1 cpd) and 100 cm for higher frequencies (2 - 8 cpd). For both monitors, the screen luminance was linearized by an 8-bit look-up table, and the mean

309 luminance was ~47 cd/m^2.

310 A drifting square-wave grating (SF = 4 cpd, contrast = full, speed = 3 cycles/s, starting
311 phase = 0°, and size = 0.4° in diameter) was first used to determine the location, eccentricity
312 (3.4^o for Monkey A, 1.7^o for Monkey B, and 1.1^o for Monkey C) and size (0.8 - 1°) of the
313 population receptive field associated with a recording field of view (FOV), as well as ocular
314 dominance columns when monocularly presented to confirm the V1 location. This fast
315 process used a 4 × objective lens mounted on the two-photon microscope and revealed no
316 cell-specific information.

317 Neuronal responses were then measured with a high-contrast (0.9) Gabor grating
318 (Gaussian-windowed sinusoidal grating) drifting at 2 cycles/s in opposite directions
319 perpendicular to the Gabor orientation. The starting phase of the drafting Gabors was always
320 0°. The Gabor grating varied at 12 orientations from 0° to 165° in 15° steps, and 6 spatial
321 frequencies from 0.25 to 8 cpd in 1-octave steps. In addition, three stimulus sizes (with
322 constant stimulus centers) were used at each spatial frequency, for two purposes. First, our
323 pilot measurements suggested very strong surround suppression with larger stimuli.
324 Therefore, comparing the responses to different stimulus sizes helped approximate the RF
325 size of each neuron that produced maximal response and least surround suppression.
326 Second, for neurons whose RF centers and the stimulus center were misaligned, the RFs of
327 some misaligned neurons might be better covered by larger stimuli. Still the RFs of additional
328 neurons might have less overlap with the stimuli. These neurons would have weaker and less
329 orientation-tuned responses because of the Gaussian-blurred stimulus edge, and would most
330 likely be filtered out during our multiple steps of selection of orientation tuned neurons (see
331 below). Specifically, the σ of the Gaussian envelope of the Gabor were 0.64λ and 0.85λ at all
332 spatial frequencies, and was additionally smaller at 0.42λ when spatial frequencies were

333 0.25 - 1 cpd, and larger at 1.06λ when spatial frequencies were 2 - 8 cpd (λ: wavelength;
334 Gabors with the same σ in wavelength unit had the same number of cycles). Here at the
335 smallest σ (0.42λ), the Gabors still had sufficient number of cycles (frequency bandwidths =
336 1 octave) (Graham, 1989), so that the actual stimulus spatial frequencies were precise at
337 nominal values. In terms of visual angle, σ = 1.68°, 2.56°, and 3.36° at 0.25 cpd; 0.84°, 1.28°,
338 and 1.68° at 0.5 cpd; 0.42°, 0.64°, and 0.85° at 1 cpd; 0.34°, 0.42°, and 0.53° at 2 cpd; 0.17°,
339 0.21°, and 0.26° at 4 cpd, and 0.08°, 0.11°, and 0.13° at 8 cpd, respectively.
340 Each stimulus was presented for 1000 ms, with an inter-stimulus interval (ISI) of 1500 ms that
341 is sufficient to allow the calcium signals back to the baseline level (Guan, Zhang, Zhang, Tang,
342 & Yu, 2020). Each stimulus condition was repeated 12 times with six repeats for each
343 opposite direction. When a stimulus was presented monocularly to one eye, the other eye
344 was covered with a translucent eye patch to reduce the impacts of short-term monocular
345 deprivation. For Monkey A, binocular recording preceded monocular recording in separate
346 days. During monocular recording contralateral and ipsilateral stimulations alternated in
347 blocks of trials with at least 10-minute breaks, during which the eye mask was taken off.
348 Recording at a specific viewing distance was completed with all trials at relevant SFs pseudo-
349 randomly presented before proceeding to the next distance. For Monkeys B and C, binocular
350 and monocular recordings were mixed and completed in two daily sessions. At a specific
351 viewing distance, all binocular trials at relevant SFs were completed first, then contralateral
352 and ipsilateral trials were completed in alternating blocks of trials with at least 10-minute
353 eye-patch-off breaks. Again, recordings at a specific viewing distance were completed before
354 proceeding to a different distance. Each block of trials typically lasted 20-25 minutes, but for
355 Monkeys A & B some blocks involving three SFs could last up to 45 minutes. The strength of
356 fluorescent signals (mean luminance of a small area) was monitored and adjusted if

357 necessary for drift of fluorescent signals. We compared the response ratios of the last 2 trials
358 over the first 2 trials for each stimulus condition in these extended blocks with ipsilateral and
359 contralateral stimulations. The respective mean ratios were 0.94 and 0.86, suggesting that
360 the recorded neuronal responses remained largely stable over extended blocks of trials.
361
362 *Two-photon imaging*
363 Two-photon imaging was performed with a Prairie Ultima IV (In Vivo) two-photon
364 microscope (Prairie Technologies) on Monkeys A and B, or a FENTOSmart two-photon
365 microscope (Femtonics) on Monkey C, and a Ti:sapphire laser (Mai Tai eHP, Spectra Physics).
366 One FOV of 850 x 850 μm^2 was selected in each animal and imaged using a 1000-nm
367 femtosecond laser under a 16 × objective lens (0.8 N.A., Nikon) at a resolution of 1.6
368 μm/pixel. Fast resonant scanning mode (32 frames per second) was chosen to obtain
369 continuous images of neuronal activity (8 frames per second after averaging every 4 frames).
370 Recording was first performed at a shallower depth, and some neurons with high brightness
371 or unique dendrite patterns were selected as landmarks. In the next daily session, the same
372 FOV at the same depth was located before recording with the help of landmarks, and the
373 depth plane was lowered if recording was performed at a deeper depth (Monkeys A & B).
374 Because of the time limit, recordings at a specific FOV/depth with monocular and binocular
375 stimulations were completed in 2-3 consecutive daily sessions, but the same neurons could
376 be precisely tracked over multiple recording sessions with the use of multiple landmark cues.
377
378 *Imaging data analysis: Initial screening of ROIs*
379 Data were analyzed with customized MATLAB codes. A normalized cross-correlation
380 based translation algorithm was used to reduce motion artifacts (Li et al., 2017). Then

fluorescence changes were associated with corresponding visual stimuli through the time sequence information recorded by Neural Signal Processor (Cerebus system, Blackrock Microsystem). By subtracting the mean of the 4 frames before stimuli onset (*F0*) from the average of the 6th-9th frames after stimuli onset (*F*) across 5 or 6 repeated trials for the same stimulus condition (same orientation, spatial frequency, size, and drifting direction), the differential image ($\Delta F = F - F0$) was obtained.

For a specific FOV at a specific recording depth, the regions of interest (ROIs) or possible cell bodies were decided through sequential analysis of 216 differential images in the order of spatial frequency (6), size (3), and orientation (12) (6 x 3 x 12 = 216). The first differential image was filtered with a band-pass Gaussian filter (size = 2-10 pixels), and connected subsets of pixels (>25 pixels, which would exclude smaller vertical neuropils) with average pixel value > 3 standard deviations of the mean brightness were selected as ROIs. Then the areas of these ROIs were set to mean brightness in the next differential image before the bandpass filtering and thresholding were performed (This measure gradually reduced the SDs of differential images and facilitated detection of neurons with relatively low fluorescence responses). If a new ROI and an existing ROI from the previous differential image overlapped, the new ROI would be on its own if the overlapping area OA < 1/4 ROI_{new}, discarded if 1/4 ROI_{new} < OA < 3/4 ROI_{new}, and merged with the existing ROI if OA > 3/4 ROI_{new}. The merges would help smooth the contours of the final ROIs. This process went on through all 512 differential images twice to select ROIs. Finally, the roundness for each ROI was calculated as:

$$Roundness = \frac{\sqrt{4\pi \times A}}{P}$$

where A was the ROI's area, and P was the perimeter. Only ROIs with roundness larger than

404 0.9, which would exclude horizontal neuropils, were selected for further analysis.

405

406 *Imaging data analysis: Orientation tuning, SF tuning, and ocular dominance*

407 The ratio of fluorescence change (*ΔF/F0*) was calculated as a neuron's response to a
408 specific stimulus condition. For a specific cell's response to a specific stimulus condition, the
409 $F0_n$ of the n-th trial was the average of 4 frames before stimulus onset, and F_n was the
410 average of 5th-8th frames after stimulus onset. $F0_n$ was then averaged across 12 trials to
411 obtain the baseline F0 for all trials (for the purpose of reducing noises in the calculations of
412 responses), and $\Delta F_n/F0 = (F_n-F0)/F0$ was taken as the neuron's response to this stimulus at
413 this trial. For a small portion of neurons (e.g., ~3% in Monkeys A, ~8% in monkey B and ~2%
414 in Monkey C) showing direction selectivity as their responses to two opposite directions
415 differed significantly ($p < 0.05$, Friedman test), the 6 trials at the preferred direction was
416 considered for calculations of $\Delta F_n/F0$ as the cell's responses to a particular stimulus. F0 was
417 still averaged over 12 trials at two opposite directions.

418 Several steps were then taken to decide whether a neuron was tuned to orientation
419 and/or spatial frequency, and if so, its ocular dominance index. For each monocular
420 condition, first the orientation, SF, and size (σ) producing the maximal response among all
421 conditions were selected. Then responses to other 11 orientations and 5 SFs were decided at
422 the selected SF and size. Second, to select orientation and/or SF tuned neurons, a non-
423 parametric Friedman test was performed to test whether a neuron's responses at 12
424 orientations or 6 SFs were significantly different from each other at least under one
425 monocular stimulation. To reduce Type-I errors, the significance level was set at $\alpha = 0.01$.
426 Third, for those showing significant orientation difference, the trial-based orientation
427 responses of each neuron were fitted with a Gaussian model with a MATLAB nonlinear least-

428 squares function: lsqnonlin:

429 $$\mathrm{R}(\theta) = a_1 2^{-(\frac{\theta-\theta_0}{\sigma})^2} + b$$

430 where R(θ) was the response at orientation θ, free parameters a_1, θ_0, σ, and b were the
431 amplitude, peak orientation, standard deviation of the Gaussian function, and minimal
432 response of the neuron, respectively. Only neurons with goodness of fit $R^2 > 0.5$ at least
433 under one stimulation condition were finally selected as orientation tuned neurons. Fourth,
434 for those showing significant SF difference, the trial-based SF responses of each neuron were
435 further fitted with a Difference-of-Gaussian model.

436 $$\mathrm{R}(sf) = a_1 e^{-(\frac{sf}{\sigma_1})^2} - a_2 e^{-\left(\frac{sf}{\sigma_2}\right)^2} + b$$

437 where R(sf) was a neuron's response at spatial frequency sf, free parameters a_1, σ_1,
438 a_2, and σ_2 were amplitudes and standard deviations of two Gaussians, respectively, and b
439 was the minimal response among 6 spatial frequencies. Only those with goodness of fit R^2 >
440 0.5 at least under one monocular stimulation were selected as SF tuned neurons.

441 The ocular dominance index (ODI) was calculated to characterize each orientation
442 and/or SF tuned neuron's eye preference: ODI = $(R_i - R_c)/(R_i + R_c)$, in which R_i and R_c were the
443 neuron's respective peak responses at the best orientation and SF to ipsilateral and
444 contralateral stimulations on the basis of data fitting. Here ODI = -1 and 1 would indicate
445 complete contralateral and ipsilateral eye preferences, respectively, and ODI = 0 would
446 indicate equal preferences to both eyes.

447

448 *Model fitting*

449 Monocular and binocular data in Fig. 4 were fitted by Eqs. 2 and 3, respectively. The
450 goodness-of-fit was indicated by a fit quality index q with a range of 0-1, which is the root

mean square deviation between the observed responses and the model normalized by the observed response mean (Busse et al., 2009):

$$q = 1 - \frac{\sqrt{\frac{\sum_{i=1}^{n}(r_i - m_i)^2}{n}}}{\bar{r}}$$

where *i* indicates the i_{th} bin, *r* indicates median response of a specific bin, and m indicates the corresponding model predictions.

Acknowledgments

This study was supported by the National Science and Technology Innovation 2030 Major Program (2022ZD0204600), Natural Science Foundation of China grants 31230030 and 31730109, and funds from Peking-Tsinghua Center for Life Sciences, Peking University.

Competing interests

None.

References

Anderson, P. A., & Movshon, J. A. (1989). Binocular combination of contrast signals. *Vision Res, 29*, 1115-1132.

Barlow, H. B., Blakemore, C., & Pettigrew, J. D. (1967). The neural mechanism of binocular depth discrimination. *J Physiol, 193*, 327-342.

Busse, L., Wade, A. R., & Carandini, M. (2009). Representation of concurrent stimuli by population activity in visual cortex. *Neuron, 64*, 931-942.

Cogan, A. I. (1987). Human binocular interaction: towards a neural model. *Vision Res, 27*, 2125-2139.

Cohn, T. E., & Lasley, D. J. (1976). Binocular vision: two possible central interactions between

signals from two eyes. *Science, 192*, 561-563.

DeSilva, H. R., & Bartley, S. H. (1930). Summation and subtraction of brightness in binocular perception. *British Journal of Psychology, 20*, 242–252.

Ding, J., Klein, S. A., & Levi, D. M. (2013). Binocular combination of phase and contrast explained by a gain-control and gain-enhancement model. *J Vis, 13*, 13.

Ding, J., & Sperling, G. (2006). A gain-control theory of binocular combination. *Proc Natl Acad Sci U S A, 103*, 1141-1146.

Dougherty, K., Cox, M. A., Westerberg, J. A., & Maier, A. (2019). Binocular Modulation of Monocular V1 Neurons. *Curr Biol, 29*, 381-391 e384.

Graham, N. (1989). *Visual Pattern Analyzers (Oxford Psychology Series, No. 16)*. New York: Oxford University Press.

Guan, S. C., Ju, N., Tao, L., Tang, S. M., & Yu, C. (2021). Functional organization of spatial frequency tuning in macaque V1 revealed with two-photon calcium imaging *Progress in Neurobiology, 205*, 102120.

Guan, S. C., Zhang, S. H., Zhang, Y. C., Tang, S., & Yu, C. (2020). Plaid detectors in macaque V1 revealed by two-photon calcium imaging. *Current Biology, 30*, 934–940.

Henriksen, S., Tanabe, S., & Cumming, B. (2016). Disparity processing in primary visual cortex. *Philos Trans R Soc Lond B Biol Sci, 371*.

Huang, C. B., Zhou, J., Zhou, Y., & Lu, Z. L. (2010). Contrast and phase combination in binocular vision. *PLoS One, 5*, e15075.

Hubel, D. H., & Wiesel, T. N. (1962). Receptive fields, binocular interaction and functional architecture in the cat's visual cortex. *J Physiol, 160*, 106-154.

Hubel, D. H., & Wiesel, T. N. (1968). Receptive fields and functional architecture of monkey striate cortex. *J Physiol, 195*, 215-243.

Ju, N., Guan, S. C., Tao, L., Tang, S. M., & Yu, C. (2021). Orientation tuning and end-stopping in macaque V1 studied with two-photon calcium imaging. *Cerebral Cortex, 31*, 2085–2097.

Li, M., Liu, F., Jiang, H., Lee, T. S., & Tang, S. (2017). Long-term two-photon imaging in awake macaque monkey. *Neuron, 93*, 1049-1057 e1043.

Li, Z. P., & Atick, J. J. (1994). Efficient Stereo Coding in the Multiscale Representation. *Network-Computation in Neural Systems, 5*, 157-174.

Lunghi, C., Burr, D. C., & Morrone, C. (2011). Brief periods of monocular deprivation disrupt

ocular balance in human adult visual cortex. *Curr Biol, 21*, R538-539.

Mitchell, B. A., Dougherty, K., Westerberg, J. A., Carlson, B. M., Daumail, L., Maier, A., & Cox, M. A. (2022). Stimulating both eyes with matching stimuli enhances V1 responses. *iScience, 25*, 104182.

Moradi, F., & Heeger, D. J. (2009). Inter-ocular contrast normalization in human visual cortex. *J Vis, 9*, 13 11-22.

Parker, A. J., Smith, J. E., & Krug, K. (2016). Neural architectures for stereo vision. *Philos Trans R Soc Lond B Biol Sci, 371*.

Pelli, D. G., & Zhang, L. (1991). Accurate control of contrast on microcomputer displays. *Vision Res, 31*, 1337-1350.

Prince, S. J., Pointon, A. D., Cumming, B. G., & Parker, A. J. (2002). Quantitative analysis of the responses of V1 neurons to horizontal disparity in dynamic random-dot stereograms. *J Neurophysiol, 87*, 191-208.

Read, J. C. A. (2021). Binocular vision and stereopsis across the animal kingdom. *Annu Rev Vis Sci, 7*, 389-415.

Welchman, A. E. (2016). The Human Brain in Depth: How We See in 3D. *Annu Rev Vis Sci, 2*, 345-376.